RESEARCH ARTICLE/REVIEW

Medinformatics 2025, Vol. 00(00) 1–9

DOI: 10.47852/bonviewMEDIN52025704



In Silico Molecular Docking and ADMET Analysis of Quinoline Compounds as Anti-SARS-CoV-2 Agents

Sidra Batool¹, Ayesha Afzal² and Muhammad Zeeshan^{1,*}

¹School of Pharmaceutical Sciences, Zhengzhou University, China

Abstract: The emergence of SARS-CoV-2 has triggered the COVID-19 pandemic, prompting urgent research into effective antiviral treatments. This manuscript focuses on the computational investigation of novel quinoline derivatives synthesized for their potential as anti-COVID-19 medications. Molecular docking simulations and computational pharmacokinetic evaluations were conducted on four quinoline derivatives (QD1–QD4) to assess their activity against SARS-CoV-2. We checked how well these derivatives bind to the SARS-CoV-2 main protease (Mpro) using molecular docking analysis. Results showed that all derivatives exhibited moderate activities against the target protein, with QD4 demonstrating the highest affinity. We also conducted ADME (absorption, distribution, metabolism, and excretion) and toxicity evaluations to evaluate the drug-likeness of the lead molecules. The derivatives' physicochemical properties and pharmacokinetic parameters indicate their potential as drug-like molecules with favorable bioavailability and low toxicity. In summary, our research suggests that these recently discovered quinoline compounds show great promise for further advancement as antiviral treatments for COVID-19.

Keywords: COVID-19, quinoline derivatives, molecular docking, ADMET, CADD

1. Introduction

The beginning of 2020 brought about a global standstill due to the emergence of a new and severe respiratory virus known as Severe Acute Respiratory Syndrome Coronavirus-2 (SARS-CoV-2) [1]. The COVID-19 pandemic originated in the Wuhan area of China in 2019 and has led to an unparalleled number of fatalities globally [2]. The International Committee on Taxonomy of Viruses officially designated this virus as SARS-CoV-2 on March 11, 2020, based on its genetic similarity to the SARS-CoV disease that occurred in 2003 [3]. Coronaviruses (CoVs) are RNA viruses with a single-stranded positive-sense RNA. They belong to the Coronaviridae family, which is classified under the order Nidovirales. Within the Coronaviridae family, they are further categorized into the subfamily Orthocoronavirinae. The Coronaviridae family is classified into four genera: alpha, beta, gamma, and delta [4, 5]. This is the most recent variant of the beta human coronavirus [6–8].

CoVs are RNA viruses with a positive-stranded RNA genome enclosed within a protective structure. They belong to the family Coronaviridae. They are classified into seven primary groups according to genome sequences and serological reactivity [9]. The CoVs included in this list are 229E (alpha coronavirus), NL63 (alpha coronavirus), OC43 (beta coronavirus), HKU1 (beta coronavirus), MERS-CoV (beta coronavirus, responsible for Middle East Respiratory Syndrome, MERS), SARS-CoV (beta coronavirus,

causing severe acute respiratory syndrome, SARS), and SARS-CoV-2 (novel coronavirus accountable for COVID-19) [10]. The genome of the SARS-CoV-2 virus is approximately 26–30 kb in length and consists of 14 open reading frames at the N-terminal and 4 structural proteins at the C-terminal [11–15]. Some CoVs may infect people, causing symptoms such as lung damage, breathing difficulties, recurring fevers, fatigue, sorrow, anxiety, and persistent memory and concentration problems. Other types of CoVs specifically target animals, causing harm to the respiratory system and olfactory epithelium of golden hamsters [16]. Early findings indicate that bats are the main source of SARS-CoV-2 transmission to humans, with pangolins serving as an intermediate host [17]. The validity of the allegations is being scrutinized in light of recent studies on the genetic and evolutionary interrelationships among CoVs found in humans, bats, and pangolins [18].

Effective antiviral candidates are being urgently investigated and repurposed to develop a potential therapy for COVID-19 to expedite the licensing process [19]. An ambitious and significant effort has been initiated to create vaccines for SARS-CoV-2 after the release of its genomic sequence. The genome contains many nonstructural and structural proteins, including spike (S), envelope (E), membrane (M), and nucleocapsid (N) proteins [20, 21]. Protease enzymes (Mpro, also known as 3C-like protease) facilitate the cleavage of viral polyproteins into functional subunits during the viral replication phase of SARS-CoV-2 and MERS [22, 23]. Therefore, proteases are a prime target for drugs against CoVs due to their lack of off-target damage [24, 25].

²PIASS College Kasur affiliated with University of Education, Pakistan

^{*}Corresponding author: Muhammad Zeeshan, School of Pharmaceutical Sciences, Zhengzhou University, China. Email: m.zeeshan@gs.zzu.edu.cn

$$N^{1}-(7\text{-chloroquinolin-4-yl})\text{ethane-1,2-diamine} \qquad N^{1}-(7\text{-chloroquinolin-4-yl})-N^{2}-(\text{pent-4-yn-1-yl})\text{ethane-1,2-diamine} \\ (\mathbf{QD1}) \qquad (\mathbf{QD2}) \\ N=N \qquad N=N \qquad N+N \qquad$$

Figure 1. Quinoline-based compounds QD1-QD4 developed specifically to test their effectiveness against SARS-CoV-2.

Thus, the inhibition of the Mpro catalytic activity by protease inhibitors obstructs the reproduction of the virus, leading to enhanced clinical results for COVID-19 and related illnesses.

Quinoline is a heterocyclic aromatic molecule consisting of a benzene ring with an abundance of electrons fused with a pyridine ring that has a deficiency of electrons. Quinolines and substituted quinolines derived from natural sources and microbes have significant biological properties. Various quinoline derivatives have been synthesized and studied for their biological effects, showing features such as antimicrobial, antiviral, anti-inflammatory, antitumor, anticancer, antidementia, antifungal, hypotensive, anti-HIV, and analgesic actions [26]. We have concentrated on computational investigations on new quinoline derivatives synthesized by the Tsogoeva group [27] for potential applications as anti-COVID medicines [28] by conducting in silico experiments against the novel coronavirus, considering the significance of quinoline nuclei in medicinal chemistry. Figure 1 displays the design considerations for substituted quinoline derivatives QD1–QD4.

2. Methodology

2.1. Dataset

To conduct this investigation, the dataset consisted of four quinoline derivatives. It has been reported that these compounds inhibit the pathogenic potential of the COVID-19 protein. Table 1 presents the optimized structures of the ligands used in the investigation, both in 2D and 3D.

2.2. Protein preparation

The PDB database (www.pdb.org) had the SARS-CoV-2 Mpro in complex with D-4-38 (PDB ID: 8GVD) [29], which was the most relevant 3D model we employed because the protein target we chose for our investigation was the SARS-CoV-2 Mpro. This structure has a resolution of 2.0A and an R-value of 0.189A. Every control was linked to a pocket that was believed to symbolize the active site. Biovia Discovery Studio 2021 was utilized for the acquisition of residues at the active site. To provide the best possible binding interactions between the ligands and the molecular targets, all

heteroatoms on the proteins, including water molecules and ligand groups, were eliminated and stored in PDB format. Subsequently, PyRx was employed to convert the proteins into macromolecules. Specified tools in the Molecular Operating Environment (MOE) were also employed to get docking scores in MOE to verify the results obtained by PyRx.

2.3. Ligand preparation

The ligands (QD1–QD4) were displayed, and their geometry optimization was examined using the Gaussian16 Rev. B.01 program at the B3LYP/6–31G (d,p) level of theory. After performing geometry optimization, three-dimensional structures were generated and saved in log format. The PyRx application then identified the Open Babel GUI [30] and used it to convert the log format into PDB format. The ligands were initially converted to the AutoDock ligand format (pdbqt) using PyRx software to achieve their best conformations with the lowest energy.

2.4. Molecular docking

The binding affinities and potential binding sites were determined by calculating the molecular docking interactions between the proteins and ligands using both the AutoDock Vina algorithm implemented within the PyRx virtual screening tool [31] and the MOE software suite. For the Vina calculations within PyRx, the docking wizard employs a stochastic gradient optimization technique to forecast binding affinities. In parallel, MOE docking was performed utilizing its induced-fit methodology: initial ligand placement was generated using the triangle matcher placement algorithm, followed by energy refinement of the resulting poses via the London dG scoring function and subsequent force field refinement. Final binding affinities (docking scores) in MOE were calculated using the GBVI/WSA dG scoring function. For each ligand-protein complex evaluated with Vina/PyRx, the docking process involved nine technical runs to ensure robustness. Similarly, MOE docking retained up to 30 poses per ligand for scoring and analysis. The docking output interaction types, including hydrogen bonds and hydrophobic interactions corresponding to the poses exhibiting the

Table 1. The ligands (QD1-QD4) under study

Compound	Name	Mol. Wt.	2D Structure	3D Optimized Structure
QD1	N1-(7- chloroquinolin-4- yl)ethane-1,2- diamine	221.69	NH ₂	
QD2	N1-(7- chloroquinolin-4- yl)-N2-(pent-4-yn- 1-yl)ethane-1,2- diamine	287.79	H N N CI	
QD3	N-(2-((7- chloroquinolin-4- yl)amino)ethyl)-N- (3-(1-(4- (morpholi- nomethyl) phenyl)-1H-1,2,3- triazol-4-yl) propyl)formamide	534.06	N=N O H N N N N N N N N N N N N N N N N N	
QD4	N-(2-((7- chloroquinolin-4- yl)amino)ethyl)-N- (3-(1-(4- (morpholino- methyl) phenyl)-1H-1,2,3- triazol-4-yl) propyl) acetamide	548.09	N=N N N N N N N N N N N N N N N N N N N	

strongest binding affinities from both Vina and MOE results, were visualized and analyzed using the Biovia Discovery Studio Visualizer 2021.

2.5. ADMET evaluation

The ADMET (Absorption, Distribution, Metabolism, Excretion, and Toxicity) properties of the four compounds (QD1–QD4) were computationally evaluated using ADMETlab 2.0, a validated platform integrating quantitative structure–activity relationship models and machine learning algorithms. The chemical structures of the compounds, provided in SMILES format, were processed by the software to generate 3D conformers and calculate over 40 descriptors, including physicochemical properties (e.g., molecular weight, logP, logD, TPSA), medicinal chemistry metrics (QED, SAscore, Fsp³), and pharmacokinetic parameters (Caco-2/MDCK permeability, P-gp substrate/inhibitor probabilities, plasma protein binding (PPB)). Toxicity endpoints such as hERG blockade, hepatotoxicity (H-HT/DILI), and

genotoxic alerts were predicted using built-in models trained on experimental datasets. Decision criteria aligned with established rules (e.g., Lipinski's Rule of Five, GSK Rule) and predefined thresholds (e.g., SAscore < 6 for synthetic feasibility, probabilities > 0.5 for toxicity risks) were applied to interpret results. Structural alerts for toxicophores, including skin sensitization and carcinogenicity, were identified through substructure screening. While ADMETlab 2.0's predictions are

Table 2. Docking scores obtained between the interactions of ligands (QD1-QD4) and protein (8GVD)

		Docking Score		
Protein	Ligand	Vina Score	MOE Score	
8GVD	QD1	-5.455	-4.994	
00 V D	QD2	-5.758	-5.333	
	QD3	-6.797	-7.334	
	QD4	-6.864	-7.314	

Table 3. ADME properties of quinoline derivatives (QD1-QD4)

Category	Parameter	Optimal Range	QD1	QD2	QD3	QD4
Physicochemical	Molecular Weight (Da)	100–600	221.07	287.12	533.23	547.25
	Volume (ų)	_	216.72	297.93	530.83	548.13
	Density (g/cm³)	_	1.02	0.96	1.01	1.00
	Hydrogen Bond Acceptors (nHA)	0–12	3	3	9	9
	Hydrogen Bond Donors (nHD)	0–7	3	2	1	1
	Rotatable Bonds (nRot)	0–11	3	7	12	12
	Rigid Bonds (nRig)	0–30	11	12	29	29
	logP	0–3	1.95	2.64	3.70	3.74
	logD (pH 7.4)	1–3	1.92	2.89	3.15	3.06
	TPSA (Ų)	0-140	50.94	36.95	88.41	88.41
Medicinal Chemistry	QED	>0.67 (Attractive)	0.836	0.606	0.277	0.301
·	SAscore	<6 (Easy synthesis)	2.04	2.43	2.92	2.78
	Fsp ³	≥0.42	0.18	0.31	0.36	0.38
	MCE-18	≥45	10.0	10.0	55.26	57.2
	Lipinski Rule	MW \leq 500; logP \leq 5; Hacc \leq 10; Hdon \leq 5	Accepted	Accepted	Accepted	Accepted
	GSK Rule	MW ≤400; logP ≤4	Accepted	Accepted	Rejected	Rejected
Absorption	Caco-2 Permeability (log unit)	>-5.15	−5.07 (•)	−4.70 (•)	-5.25 (•)	−5.33 (•)
•	MDCK Permeability ($\times 10^{-6}$ cm/s)	>20 (High)	0.007 (Low)	0.015 (Medium)	0.017 (Medium)	0.028 (Medium)
	P-gp Substrate Probability	Low desired	0.985 (•)	0.954 (•)	0.003 (•)	0.006 (•)
	HIA+ Probability	Low desired	0.20	0.003	0.022	0.005
Distribution	Plasma Protein Binding (%)	<90	48.10	90.54	91.77	95.82
	BBB Penetration Probability	Target-dependent	0.45	0.99 (•)	0.87	0.83
	Fraction Unbound (%)	>20 (High)	48.36	4.87	7.44	4.44
Metabolism	CYP3A4 Inhibitor Probability	Low desired	0.14	0.28	0.89 (•)	0.90 (•)
	CYP2D6 Inhibitor Probability	Low desired	0.55	0.94 (•)	0.79 (•)	0.75 (•)
Excretion	Clearance (mL/min/kg)	<5 (Low)	6.21 (Moderate)	4.28 (Low)	5.30 (Moderate)	4.68 (Low)
	Half-life >3h Probability	High desired	0.36	0.23	0.11	0.14
Toxicity	hERG Blockers Probability	Low desired	0.64 (•)	0.90 (•)	0.81 (•)	0.76 (•)
•	Hepatotoxicity (H-HT)	Low desired	0.79 (•)	0.94 (•)	0.94 (•)	0.98 (•)
	AMES Toxicity Probability	Low desired	0.84 (•)	0.66 (•)	0.08	0.03
Environmental Toxicity Bioconcentration Factor		Lower desired	0.67	0.90	1.10	1.25
Tox21 Pathways AhR Activation Probability		Low desired	0.95 (•)	0.95 (•)	0.62 (•)	0.64 (•)
Toxicophore Alerts	Skin Sensitization	0 alerts desired	0	3	2	2
•	Genotoxic Carcinogenicity	0 alerts desired	1	1	1	1

Note: (•) Indicates a parameter outside the optimal range or posing a risk.

HIA+: Human Intestinal Absorption (probability of absorption <30%).

TPSA: Topological Polar Surface Area; QED: Quantitative Estimate of Drug-likeness; SAscore: Synthetic Accessibility Score.

CYP: Cytochrome P450; P-gp: P-glycoprotein; BBB: Blood-Brain Barrier.

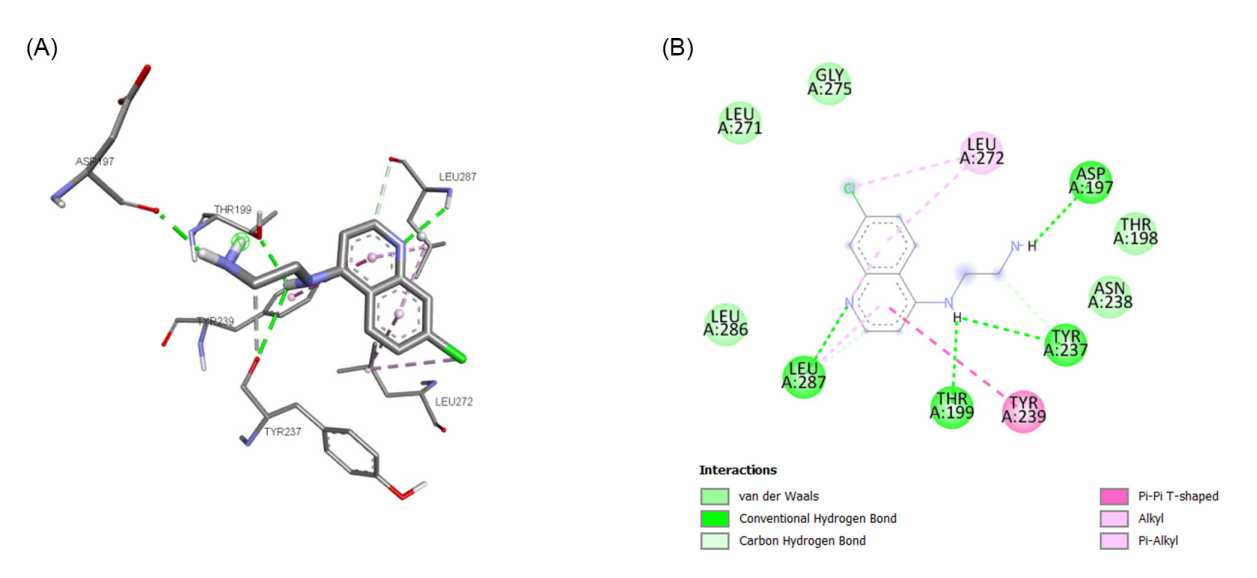


Figure 2. QD1 docked in SARS-CoV-2 (8DVG): (A) The residues interacting with QD1 in the pocket view of 8GVD. (B) 2D schematic diagram illustrating a docking model of interactions between QD1 and an amino acid with hydrogen bonds in 8DVG.

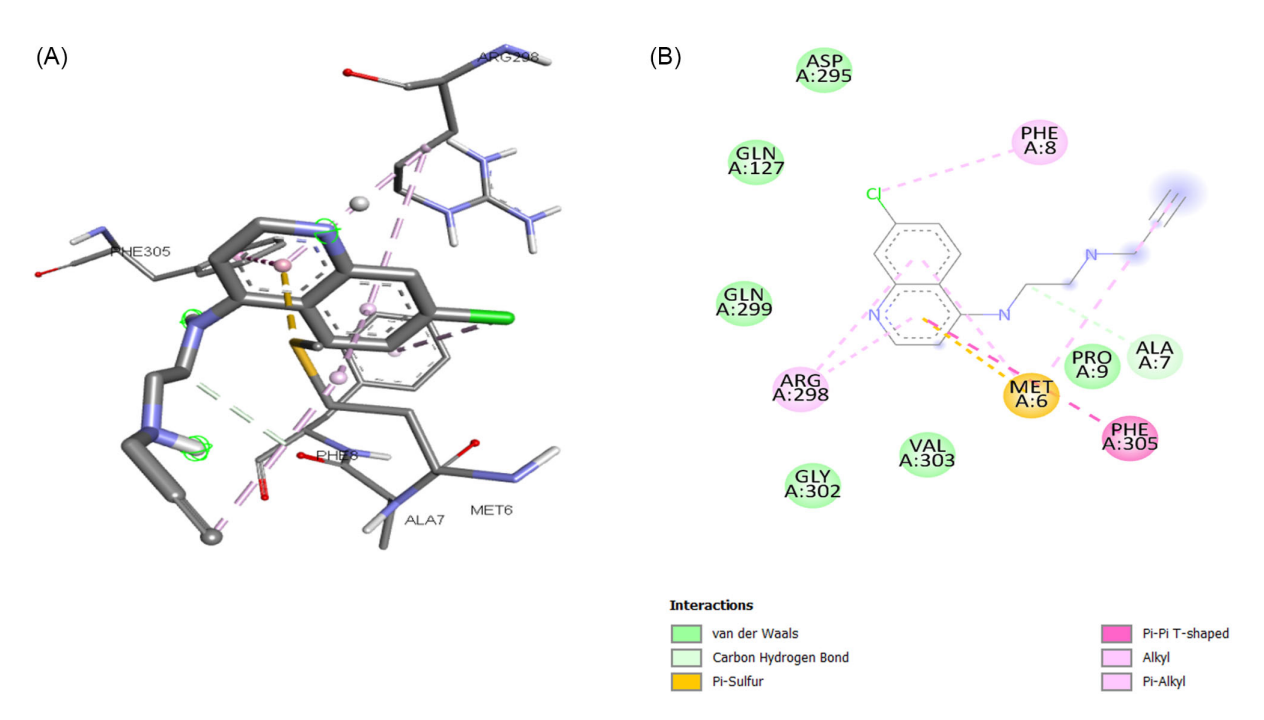


Figure 3. QD2 docked in SARS-CoV-2 (8DVG): (A) The residues interacting with QD2 in the pocket view of 8GVD. (B) 2D schematic diagram illustrating a docking model of interactions between QD2 and an amino acid with hydrogen bonds in 8DVG.

robust due to its training on diverse experimental data, the computational findings are intended for preliminary prioritization and require experimental validation to address biological complexities. This approach provided a rapid, cost-effective framework to assess drug-likeness and safety, guiding further optimization of QD1–QD4.

3. Results and Discussion

The objective of the research was to predict the affinities of four ligands, which have been reported to have antiviral activity, for the

COVID-19 Mpro target protein. The lower the value of the binding energy, the more applicable and useful it would be. How effectively a chemical substance functions as a drug is largely dependent on its ADME (absorption, distribution, metabolism, and excretion) characteristics. ADME properties can be enhanced through the rigorous process of drug design and testing, hence reducing the risk of pharmacokinetics-related failures during clinical stages. Research has demonstrated that including ADME early on in the clinical drug development process can lower attrition rates. This led to the evaluation of four quinoline derivatives' early-stage ADME properties through the use of the Admetlab 2 online tool.

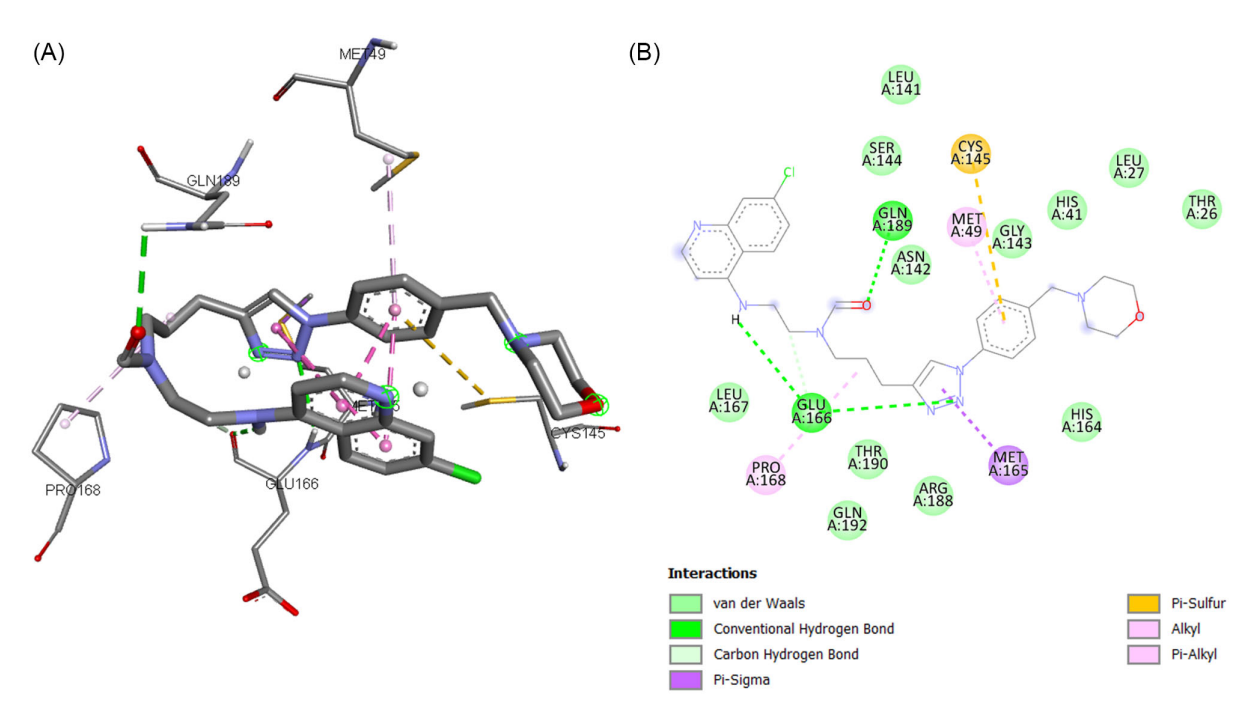


Figure 4. QD3 docked in SARS-CoV-2 (8DVG): (A) The residues interacting with QD3 in the pocket view of 8GVD. (B) 2D schematic diagram illustrating a docking model of interactions between QD3 and an amino acid with hydrogen bonds in 8DVG.

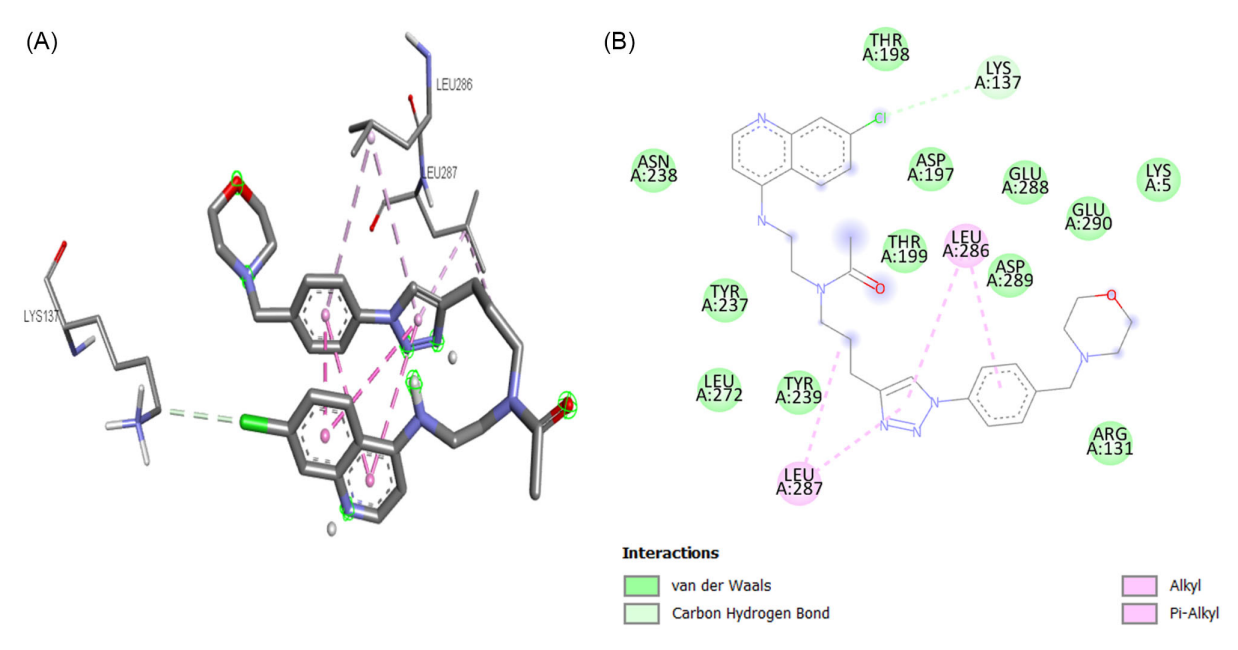


Figure 5. QD4 docked in SARS-CoV-2 (8DVG): (A) The residues interacting with QD4 in the pocket view of 8GVD. (B) 2D schematic diagram illustrating a docking model of interactions between QD4 and an amino acid with hydrogen bonds in 8DVG.

3.1. Molecular docking analysis

Quinoline derivatives were shown to have anti-SARS-CoV-2 characteristics, which were confirmed by molecular docking analysis. The SARS-CoV-2 target, with the PDB ID 8GVD, was compared against four ligands to ascertain potential binding interactions between the protein and the quinoline derivatives. A total of nine poses were acquired and assessed for all docking

simulations. Quinoline derivatives were successfully docked to the 8GVD, and interaction mechanisms were identified for each docking score. This study evaluated the inhibitory effects of four ligand molecules on 8GVD. Protein (8GVD) and drug molecules (ligands) exhibit distinct behaviors during docking, which are influenced by factors such as hydrogen bonding, hydrophobic interactions, van der Waals forces, and ionic interactions. The ligand with the highest docking score exhibits the greatest

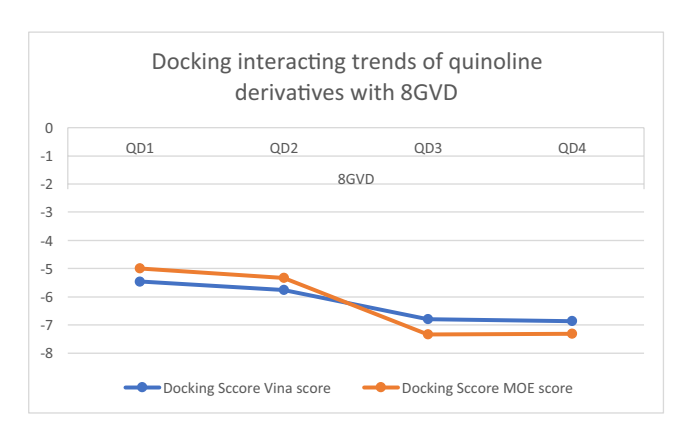


Figure 6. Graphical representation of docking scores of ligands (QD1–QD4) with 8GVD.

stability (Table 2). Molecular docking requires more than just the binding energy and RMSD data. Additionally important are molecular interactions such as van der Waals forces, hydrophobic bonds, ionic bonds, and hydrogen bonds.

It was also observed that there is a connection between specific amino acids and how ligands and proteins interact. QD1 (N1-(7-chloroquinolin-4-yl)ethane-1,2-diamine) demonstrated binding affinities of -4.994 kcal/mol in MOE and -5.455 kcal/mol in Vina by forming H-bonds with Leu-287, Asp-197, and Thr-199 in the active site of 8GVD. A little pi-pi stacking interaction with Tyr-239 was seen in QD1 (Figure 2).

In the active site of 8GVD, QD2 (N1-(7-chloroquinolin-4-yl)-N2-(pent-4-yn-1-yl)ethane-1,2-diamine) forms carbon-H-bonds with Ala-7, with a binding energy of -5.3332 kcal/mol in MOE and -5.758 kcal/mol in Vina (Figure 3). In addition, QD2 made one pi-sulfur bond with Met-6 and pi-alkyl interactions with Arg-298.

QD3 (N-(2-((4-yl)amino(7-chloroquinolin)ethyl)-N-(3-(1-(4-(morpholinomethyl)phenyl)-1H-1,2,3-triazol-4-yl)propyl)formamide), which formed pi-alkyl interactions with Glu-166 and Gln-189 in the 8GVD active site, demonstrated strong binding with a binding affinity of -7.334 kcal/mol in MOE and in Vina -6.797 kcal/mol. Figure 4 shows some of the pi-sulfur interactions that were seen between Cys-149 and QD3.

QD4 (N-(2-((7-chloroquinolin-4-yl)amino)ethyl)-N-(3-(1-(4-(morpholinomethyl)phenyl))-1H-1,2,3-triazol-4-yl)propyl)acetamide) was able to bind significantly, which generated a binding affinity of -7.314 kcal/mol in MOE and -6.864 kcal/mol in Vina by forming H-bonds with Leu-286 and Leu-287 in the 8GVD active site (Figure 5).

Figure 6 shows the graphical comparison of docking scores of ligands and target protein taken from AutoDock Vina and MOE.

The docking results show that all derivatives have moderate activities against the target protein, whereas QD4 has the highest affinity among all the derivatives.

3.2. ADME and toxicity results

The ADMET profiles of four compounds (QD1–QD4) were systematically evaluated using ADMETlab 2.0 to assess their drug-likeness and safety. Key physicochemical properties revealed distinct differences among the compounds. QD1 (221.07 Da) and QD2 (287.12 Da) exhibited molecular weights within the optimal range (100–500 Da), aligning with Lipinski's Rule of Five and suggesting favorable oral bioavailability. In contrast, QD3 (533.23 Da) and QD4 (547.25 Da) exceeded this threshold, potentially

compromising their absorption and permeability. Lipophilicity trends further differentiated the compounds: QD1 (logP = 1.95) and QD2 (logP = 2.64) fell within the desirable range (0–3), while QD3 (logP = 3.70) and QD4 (logP = 3.74) demonstrated elevated lipophilicity, which may increase off-target binding and toxicity risks. Topological polar surface area (TPSA) values (36.95–88.41 Ų) for all compounds were within the optimal range (0–140 Ų), indicating adequate membrane permeability.

In medicinal chemistry parameters, QD1 exhibited strong drug-likeness with a high QED score (0.836), whereas QD2 (0.606), QD3 (0.277), and QD4 (0.301) scored lower, reflecting structural complexity or suboptimal physicochemical balance. Synthetic accessibility scores (SAscore: 2.04–2.92) for all compounds were below 6, suggesting feasible synthesis. However, Fsp³ values for QD1 (0.18) and QD2 (0.31) fell below the preferred threshold (\geq 0.42), indicating potential solubility challenges, while QD3 (0.36) and QD4 (0.38) showed marginal improvement.

Absorption and distribution profiles highlighted critical differences. QD1 and QD2 displayed acceptable Caco-2 permeability (>-5.15), whereas QD3 and QD4 were borderline, raising concerns about intestinal absorption. P-glycoprotein (P-gp) substrate probabilities were notably high for QD1 (0.985) and QD2 (0.954), suggesting susceptibility to efflux-mediated poor bioavailability. Conversely, QD3 (0.003) and QD4 (0.006) showed negligible P-gp interaction, a favorable trait. PPB exceeded 90% for QD3 (91.77%) and QD4 (95.82%), likely reducing free drug availability and therapeutic efficacy. QD2 demonstrated a high probability of blood-brain barrier penetration (BBB+=0.99), which may be advantageous for central nervous system targets but poses risks for unintended neurotoxicity.

Metabolism data revealed significant cytochrome P450 (CYP) interactions. QD3 and QD4 exhibited high inhibition probabilities for CYP2D6 (e.g., QD3: 0.788) and CYP3A4 (e.g., QD4: 0.904), indicating potential drug–drug interactions. Excretion parameters indicated moderate-to-low clearance (4.28–6.21 mL/min/kg) for all compounds, suggesting prolonged systemic exposure. Half-life probabilities (T1/2 >3h: <0.3) implied short elimination times, necessitating frequent dosing regimens.

Toxicity assessments raised critical safety concerns. All compounds showed high probabilities of hERG channel blockade (QD1: 0.64; QD2: 0.90; QD3: 0.81; QD4: 0.76), signaling cardiac toxicity risks. Hepatotoxicity markers (H-HT: 0.79–0.98; DILI: 0.75–0.97) were elevated across the series, with QD4 displaying the highest likelihood of liver injury. Environmental toxicity parameters, such as bioconcentration factors (e.g., QD4: 1.25), and structural alerts for skin sensitization (2–3 alerts per compound) further underscored safety liabilities. Tox21 pathway analysis highlighted strong aryl hydrocarbon receptor (AhR) activation (0.62–0.95), associated with xenobiotic metabolism and carcinogenic potential.

In conclusion, QD1 and QD2, despite favorable physicochemical properties, face challenges related to P-gp-mediated efflux and toxicity. QD3 and QD4, while avoiding P-gp interactions, exhibit poor drug-likeness, significant CYP inhibition, and pronounced safety risks. Structural optimization to reduce lipophilicity, mitigate hERG and hepatotoxicity liabilities, and improve metabolic stability is essential for advancing these compounds toward preclinical development. Further in vitro and in vivo studies are warranted to validate these computational predictions.

4. Conclusion

Computational investigations have identified promising quinoline derivatives, synthesized by the Tsogoeva group, as potential candidates for anti-COVID-19 medications. Molecular docking analyses revealed moderate binding affinities of these derivatives to the SARS-CoV-2 main protease (Mpro), with QD4 exhibiting the highest affinity. Furthermore, ADME and toxicity evaluations demonstrated favorable drug-like properties, suggesting these compounds have potential for further development. The results presented here contribute valuable insights into the search for effective treatments against COVID-19. However, further experimental studies, including in vitro and in vivo evaluations, are warranted to validate the antiviral activity and safety profile of these quinoline derivatives. Additionally, optimization of the chemical structures and refinement of the pharmacokinetic properties could enhance their efficacy and therapeutic potential. Overall, the findings from this study underscore the importance of computational approaches in drug discovery and highlight the potential of quinoline derivatives as promising candidates for combating the COVID-19 pandemic. Further research and development efforts are essential to accelerate the translation of these findings into clinically viable treatments for COVID-19 patients.

Acknowledgment

We express our gratitude to Dr. Zarif Gul for his wonderful teaching and moral support.

Ethical Statement

This study does not contain any studies with human or animal subjects performed by any of the authors.

Conflicts of Interest

The authors declare that they have no conflicts of interest to this work.

Data Availability Statement

Data sharing is not applicable to this article as no new data were created or analyzed in this study.

Author Contribution Statement

Sidra Batool: Conceptualization, Methodology, Software, Validation, Formal analysis, Investigation, Resources, Data curation, Writing – original draft, Writing – review & editing, Visualization, Project administration. Ayesha Afzal: Methodology, Software, Validation, Formal analysis, Investigation, Resources, Data curation, Writing – original draft, Writing – review & editing, Visualization. Muhammad Zeeshan: Conceptualization, Validation, Resources, Data curation, Writing – original draft, Writing – review & editing, Visualization, Supervision, Project administration, Funding acquisition.

References

- [1] Acter, T., Uddin, N., Das, J., Akhter, A., Choudhury, T. R., & Kim, S. (2020). Evolution of severe acute respiratory syndrome coronavirus 2 (SARS-CoV-2) as coronavirus disease 2019 (COVID-19) pandemic: A global health emergency. *Science of the Total Environment*, 730, 138996. https://doi.org/10.1016/j.scitotenv.2020.138996
- [2] Sifuentes-Rodríguez, E., & Palacios-Reyes, D. (2020). COVID-19: The outbreak caused by a new coronavirus.

- Boletin Medico del Hospital Infantil de Mexico, 77(2), 47–53. https://doi.org/10.24875/bmhim.20000039
- [3] Gorbalenya, A. E., Baker, S. C., Baric, R. S., de Groot, R. J., Drosten, C., Gulyaeva, A. A., ..., & Ziebuhr, J. (2020). Severe acute respiratory syndrome-related coronavirus: The species and its viruses—A statement of the Coronavirus Study Group. *BioRxiv*. https://doi.org/10.1101/2020.02.07.937862
- [4] Yang, D., & Leibowitz, J. L. (2015). The structure and functions of coronavirus genomic 3' and 5' ends. Virus Research, 206, 120–133. https://doi.org/10.1016/j.virusres. 2015.02.025
- [5] Malik, Y. A. (2020). Properties of coronavirus and SARS-CoV-2. *The Malaysian Journal of Pathology*, 42(1), 3–11.
- [6] Buonaguro, L., Tagliamonte, M., Tornesello, M. L., & Buonaguro, F. M. (2020). SARS-CoV-2 RNA polymerase as target for antiviral therapy. *Journal of Translational Medicine*, 18(1), 185. https://doi.org/10.1186/s12967-020-02355-3
- [7] Wang, Q., Wu, J., Wang, H., Gao, Y., Liu, Q., Mu, A., ..., & Rao, Z. (2020). Structural basis for RNA replication by the SARS-CoV-2 polymerase. *Cell*, 182(2), 417–428. https://doi.org/10.1016/j.cell.2020.05.034
- [8] Zhao, Z., & Bourne, P. E. (2020). Structural insights into the binding modes of viral RNA-dependent RNA polymerases using a function-site interaction fingerprint method for RNA virus drug discovery. *Journal of Proteome Research*, 19(11), 4698–4705. https://doi.org/10.1021/acs.jproteome.0c00623
- [9] Gohar, U. F., Iqbal, I., Shah, Z., Mukhtar, H., & Zia-Ul-Haq, M. (2021). COVID-19: recent developments in therapeutic approaches. In Alternative Medicine Interventions for COVID-19, 249–274. https://doi.org/10.1007/978-3-030-67989-7
- [10] Leao, J. C., Gusmao, T. P. D. L., Zarzar, A. M., Leao Filho, J. C., Barkokebas Santos de Faria, A., Morais Silva, I. H., ..., & Carvalho, A. D. A. T. (2022). Coronaviridae—Old friends, new enemy! *Oral Diseases*, *28*, 858–866. https://doi.org/10.1111/odi.13447
- [11] Gao, Y., Yan, L., Huang, Y., Liu, F., Zhao, Y., Cao, L., ..., & Rao, Z. (2020). Structure of the RNA-dependent RNA polymerase from COVID-19 virus. *Science*, *368*(6492), 779–782. https://doi.org/10.1126/science.abb7498
- [12] Yin, W., Mao, C., Luan, X., Shen, D. D., Shen, Q., Su, H., ..., & Xu, H. E. (2020). Structural basis for inhibition of the RNAdependent RNA polymerase from SARS-CoV-2 by remdesivir. *Science*, 368(6498), 1499–1504. https://doi.org/10.1126/ science.abc1560
- [13] Jiang, Y., Yin, W., & Xu, H. E. (2021). RNA-dependent RNA polymerase: Structure, mechanism, and drug discovery for COVID-19. *Biochemical and Biophysical Research Communications*, 538, 47–53. https://doi.org/10.1016/j.bbrc. 2020.08.116
- [14] Wu, F., Zhao, S., Yu, B., Chen, Y. M., Wang, W., Song, Z. G., ..., & Zhang, Y. Z. (2020). A new coronavirus associated with human respiratory disease in China. *Nature*, *579*(7798), 265–269. https://doi.org/10.1038/s41586-020-2008-3
- [15] Shereen, M. A., Khan, S., Kazmi, A., Bashir, N., & Siddique, R. (2020). COVID-19 infection: Emergence, transmission, and characteristics of human coronaviruses. *Journal of Advanced Research*, 24, 91–98. https://doi.org/10.1016/j.jare.2020.03.005
- [16] Frere, J. J., Serafini, R. A., Pryce, K. D., Zazhytska, M., Oishi, K., Golynker, I., ..., & Tenoever, B. R. (2022). SARS-CoV-2 infection in hamsters and humans results in lasting and unique

- systemic perturbations after recovery. *Science Translational Medicine*, 14(664), eabq3059. https://doi.org/10.1126/scitranslmed.abq3059
- [17] Chakraborty, C., Bhattacharya, M., Nandi, S. S., Mohapatra, R. K., Dhama, K., & Agoramoorthy, G. (2022). Appearance and re-appearance of zoonotic disease during the pandemic period: long-term monitoring and analysis of zoonosis is crucial to confirm the animal origin of SARS-CoV-2 and monkeypox virus. *Veterinary Quarterly*, 42(1), 119–124. https://doi.org/10.1080/01652176.2022.2086718
- [18] Liu, P., Jiang, J. Z., Wan, X. F., Hua, Y., Li, L., Zhou, J., ..., & Chen, J. (2020). Are pangolins the intermediate host of the 2019 novel coronavirus (SARS-CoV-2)? *PLoS Pathogens*, 16(5), e1008421. https://doi.org/10.1371/journal.ppat.1009664
- [19] Ancy, I., Sivanandam, M., & Kumaradhas, P. (2021). Possibility of HIV-1 protease inhibitors-clinical trial drugs as repurposed drugs for SARS-CoV-2 main protease: a molecular docking, molecular dynamics and binding free energy simulation study. *Journal of Biomolecular Structure* and Dynamics, 39(15), 5368–5375. https://doi.org/10.1080/ 07391102.2020.1786459
- [20] Du, L., He, Y., Zhou, Y., Liu, S., Zheng, B. J., & Jiang, S. (2009). The spike protein of SARS-CoV—a target for vaccine and therapeutic development. *Nature Reviews Microbiology*, 7(3), 226–236. https://doi.org/10.1038/nrmicro2090
- [21] Ghosh, R., Chakraborty, A., Biswas, A., & Chowdhuri, S. (2022). Computer aided identification of potential SARS CoV-2 main protease inhibitors from diterpenoids and biflavonoids of *Torreya nucifera* leaves. *Journal of Biomolecular Structure and Dynamics*, 40(6), 2647–2662. https://doi.org/10.1080/07391102.2020.1841680
- [22] Bhardwaj, V. K., Singh, R., Das, P., & Purohit, R. (2021). Evaluation of acridinedione analogs as potential SARS-CoV-2 main protease inhibitors and their comparison with repurposed anti-viral drugs. *Computers in Biology and Medicine*, 128, 104117. https://doi.org/10.1016/j.compbiomed.2020.104117
- [23] Singh, R., Bhardwaj, V., & Purohit, R. (2021). Identification of a novel binding mechanism of quinoline based molecules with lactate dehydrogenase of Plasmodium falciparum. *Journal of Biomolecular Structure and Dynamics*, 39(1), 348–356. https://doi.org/10.1080/07391102.2020.1711809
- [24] Ghosh, R., Chakraborty, A., Biswas, A., & Chowdhuri, S. (2021). Identification of alkaloids from *Justicia adhatoda* as potent SARS CoV-2 main protease inhibitors: An in silico

- perspective. *Journal of Molecular Structure*, 1229, 129489. https://doi.org/10.1016/j.molstruc.2020.129489
- [25] Sharma, J., Bhardwaj, V. K., Singh, R., Rajendran, V., Purohit, R., & Kumar, S. (2021). An in-silico evaluation of different bioactive molecules of tea for their inhibition potency against non structural protein-15 of SARS-CoV-2. Food Chemistry, 346, 128933. https://doi.org/10.1016/j.foodchem.2020.128933
- [26] Amer, A., El-Eraky, W. I., & Mahgoub, S. (2018). Synthesis, characterization and antimicrobial activity of some novel quinoline derivatives bearing pyrazole and pyridine moieties. Egyptian Journal of Chemistry, 61(Conference issue (14th Ibn Sina Arab Conference on Heterocyclic Chemistry and its Applications (ISACHC 2018), 30 March-2 April 2018, Hurghada, Egypt)), 1–8. https://doi.org/10.21608/ejchem. 2018.3941.1345
- [27] Herrmann, L., Hahn, F., Wangen, C., Marschall, M., & Tsogoeva, S. B. (2022). Anti-SARS-CoV-2 inhibitory profile of new quinoline compounds in cell culture-based infection models. *Chemistry—A European Journal*, 28(4), e202103861. https://doi.org/10.1002/chem.202103861
- [28] Aldahham, B. J., Al-Khafaji, K., Saleh, M. Y., Abdelhakem, A. M., Alanazi, A. M., & Islam, M. A. (2022). Identification of naphthyridine and quinoline derivatives as potential Nsp16-Nsp10 inhibitors: a pharmacoinformatics study. *Journal of Biomolecular Structure and Dynamics*, 40(9), 3899–3906. https://doi.org/10.1080/07391102.2020.1851305
- [29] Liu, M., Li, J., Liu, W., Yang, Y., Zhang, M., Ye, Y., ..., & Huang, H. (2023). The S1'-S3' pocket of the SARS-CoV-2 main protease is critical for substrate selectivity and can be targeted with covalent inhibitors. *Angewandte Chemie International Edition*, 62(41), e202309657. https://doi.org/10.1002/anie.202309657
- [30] O'Boyle, N. M., Banck, M., James, C. A., Morley, C., Vandermeersch, T., & Hutchison, G. R. (2011). Open Babel: An open chemical toolbox. *Journal of Cheminformatics*, 3(1), 33. https://doi.org/10.1186/1758-2946-3-33
- [31] Dallakyan, S., & Olson, A. J. (2014). Small-molecule library screening by docking with PyRx. In *Chemical biology: Methods and protocols* (pp. 243–250). New York, NY: Springer New York. https://doi.org/10.1007/978-1-4939-2269-7_19

How to Cite: Batool, S., Afzal, A., & Zeeshan, M. (2025). In Silico Molecular Docking and ADMET Analysis of Quinoline Compounds as Anti-SARS-CoV-2 Agents. *Medinformatics*. https://doi.org/10.47852/bonviewMEDIN52025704